A Study of a TBA Lattice for the Pohang Light Source

Kwanghee Nam and Jinhyuk Choi
Pohang Accelerator Laboratory
Pohang P.O.Box 125, Kyungbuk 790-600
Republic of Korea

A triple bend achromat lattice is chosen for the 2~2.5 GeV Pohang Light Source. Flexibility obtained by employing 12 quadrupoles per cell leads to the design of a hybrid type lattice which has both high and low horizontal betatron values in the insertion device sections. A conventional 12 period TBA lattice functions are also obtained with a different family of quadrupole strengths.

PLS Magnet Lattice

The Pohang Light Source is a $2 \sim 2.5$ GeV synchrotron light source whose storage ring is made of 6 or 12 superperiod triple bend achromat magnet lattice. The circumference is 280.56 m, the RF frequency is 500.087 MHz, and the corresponding harmonic number is 468 ($= 2^2 \cdot 3^2 \cdot 13$).

PLS storage ring magnet lattice has 12 quadrupole magnets per cell. Triplets of quadrupoles in the insertion device (ID) sections are used for ID matching, and triplets of quadrupoles in the achromat sections are used for the suppression of dispersion function and phase advance control. A conventional 12 period magnet lattice function and its properties are shown in appendix.

Compared with other TBA lattices such as LBL, SRRC, BESSY, the PLS magnet lattice utilizes a larger number of quadrupoles, which makes it possible to produce hybrid type lattice functions. That is, a combination of 12 quadrupoles strengths leads to a lattice design with six high and six low horizontal betatron (β_x) values at the ID symmetry points. The high β_x location as used for undulators for the homogeneity of the spectrum, while the low β_x locations are used for wigglers for the minimum disturbance to the lattice. Lattice function in Figure 1 shows such a hybrid type configuration, and its parameters are listed in Table 1. The magnet lattice parameters are listed in Table 2.

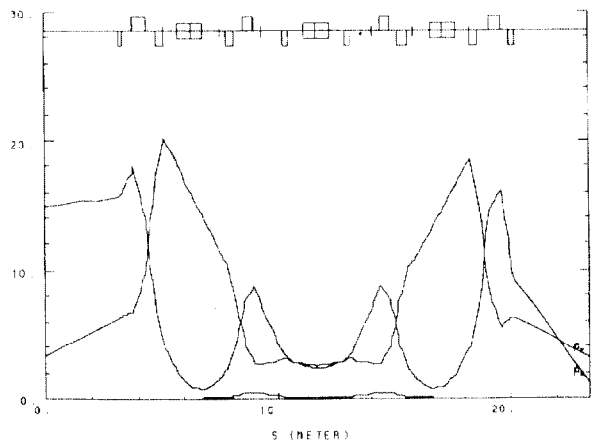

Figure 1. A hybrid type lattice functions over half cell.

Lattice Type	TBA
Nominal Energy	2-2.5 (GeV)
Superperiod	6
Circumference	280.56 (m)
Mean Radius	44.65 (m)
Harmonic Number	468
RF Frequency	500.082 (MHz)
Natural Emittance	13.3 ($nm \cdot rad$)
Natural Chromaticity (h/v)	-29.94/-18.63
Betatron Tunes (h/v)	15.28/9.18
Beta Functions (h/v)	
Maximum	18/20.2 (m)
Minimum	0.75/2.6 (m)
At ID symmetry point (high/low)	15/3.3, 1.3/3.1 (m)
Beam Size at ID Sym. Pt. (high/low)	
Horizontal, σ_x	0.45/0.13 (mm)
Vertical ($r = 1$), σ_y	0.15/0.14(mm)
Energy Spread, σ_E	0.00068
Maximum Dispersion	0.506 (m)
Momentum Compaction	0.001921
Dipole Length	1.1(m)
Dipole Field	1.06/1.32(T)
Bending Radius	6.303 (m)

Table 1. Major storage ring parameters at 2 GeV.

Chromaticity Correction

Two pairs of sextupoles (SD, SF) = ($-6.13\,\mathrm{m}^{-2}$, $4.59\,\mathrm{m}^{-2}$), (SDM, SFM) = ($-7.08\,\mathrm{m}^{-2}$, $5.77\,\mathrm{m}^{-2}$) are used for chromaticity correction. A plot of tune versus momentum is shown in Figure 2, and a plot of tune versus amplitudes is shown in Figure 3 where the vertical tune is calculated when the horizontal amplitude is fixed at $N_x = 30$. Figure 4 shows the dynamic aperture without error at the point of high β_x ID symmetry point.

For the analysis of multipole error sensitivity, we utiliz the multipole error listed in Table 3. At this time, we use a field expansion like

$$B_y(x,\phi) = B\rho \sum_n \frac{k_n x^n}{n!} \cos\{(n+1)\phi + \delta\},$$

Element	Length (m)	Strength
L0	3.18	
Q1	0.24	-0.5431 (m^{-2})
L1	0.36	
Q2	0.53	1.3893 (m^{-2})
L2	0.46	
Q3	0.35	-1.6886 (m^{-2})
L3	0.60	
B	1.1	6.303 (m)
L41	0.63	
SD	0.16	-6.1307 (m^{-2})
L42	0.18	
Q4	0.35	-1.3494 (m^{-2})
L5	0.34	
Q5	0.53	1.8205 (m^{-2})
L61	0.16	
SF	0.16	4.5298 (m^{-2})
L62	0.91	
Q6	0.24	-1.1578 (m^{-2})
L7	0.66	
B	1.1	6.303 (m)
L7	0.66	
Q6M	0.24	-1.2047 (m^{-2})
L62	0.91	
SFM	0.16	5.7686 (m^{-2})
L61	0.16	
Q5M	0.53	1.8418 (m^{-2})
L5	0.34	
Q4M	0.35	-1.4100 (m^{-2})
L42	0.18	
SDM	0.16	-7.0830 (m^{-2})
L41	0.63	
B	1.1	6.303 (m)
L3	0.60	
Q3M	0.35	-1.8624 (m^{-2})
L2	0.46	
Q2M	0.53	2.0521 (m^{-2})
L1	0.36	
Q1M	0.24	-1.3896 (m^{-2})
L0	3.18	

Table 2. Magnet lattice parameters for a hybrid configuration.

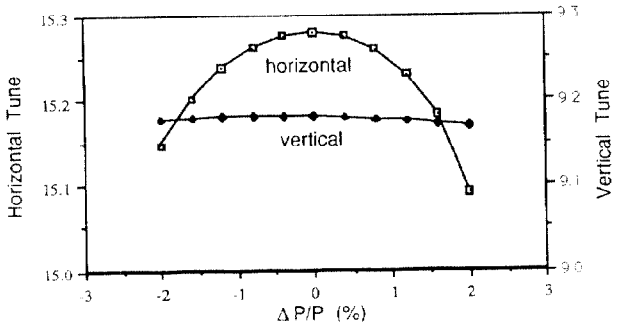

Figure 2. Tune shifts versus momentum

where k_n is the multipole amplitude, ϕ is the angle about the beam axis, and δ is an offset angle axis, which measures the skew with respect to the normal orientation. Figure 5 shows the dynamic aperture with all errors in Table 3.

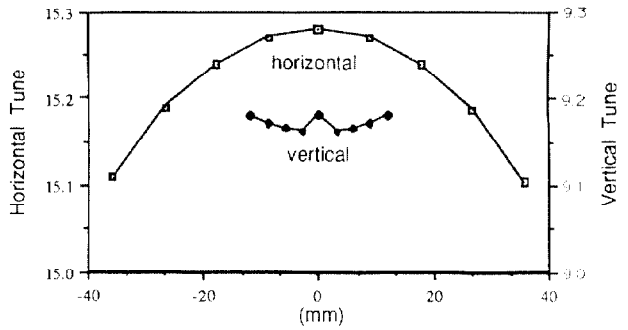

Figure 3. Horizontal tune for $N_y = 0$ versus horizontal amplitude and vertical tune for $N_x = 30$ versus vertical amplitude.

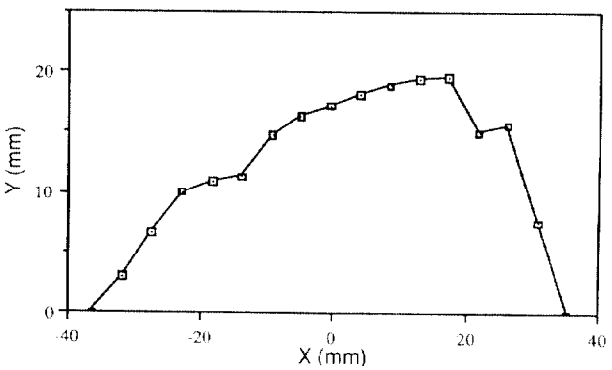

Figure 4. Dynamic aperture without error.

	$k_1 l$	$k_2 l$	$k_3 l$	$k_4 l$	$k_5 l$	$k_9 l$
Systematic						
Dipoles	$1.7 \cdot 10^{-5}$	-0.087	0.0	1743	0.0	0.0
Quadrupoles	$5 \cdot 10^{-4}$	0.0	0.0	0.0	$-1.5 \cdot 10^{5}$	$1.5 \cdot 10^{12}$
Random						
Dipoles	$3.4 \cdot 10^{-5}$	0.174	26.1	174.0	0.0	0.0
Quadrupoles	10^{-3}	0.1	15.0	300.0	$3 \cdot 10^{4}$	$5 \cdot 10^{11}$

Table 3. Input parameters for multipole error simulations.

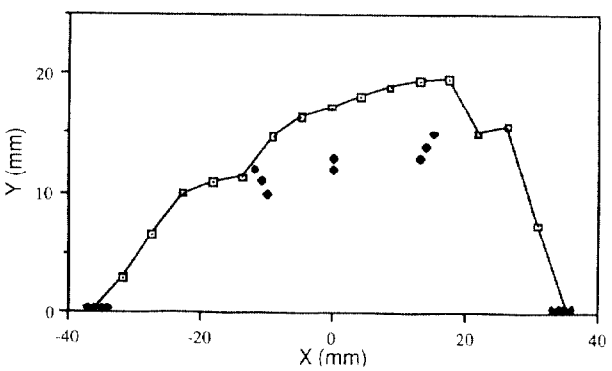

Figure 5. Dynamic aperture with all multipole errors listed in Table 3 for 10 different machines

Effects of Insertion Devices

Insertion devices not only break the linear optics of the lattice, but also introduce higher order field components that may excite non-systematic resonances. In most insertion devices, closed paths are wiggled in the horizontal direction through the vertical field variation, so that it results in an vertical focussing. Hence, only the vertical tune changes with a horizontally wiggling insertion device. For the recovery of the breaks in linear optics, techniques of α-matching and tune matching are utilized.

It is possible to obtain α and tune matching by readjusting three insertion quadrupoles Q1, Q2, Q3. Table 5 shows the values of Q1, Q2, Q3 before and after α and tune matching for the insertion devices listed in Table 4. Figure 6 shows the dynamic apertures when one wiggler and one undulator in Table 4 are inserted, respectively. For the particle tracking, we have used L. Smith's approach of RACETRACK. The number of integration steps is 10 for the undulator, and 20 for the wiggler. In both cases particles are tracked for100 turns.

	Undulator	Wiggler
Field Parameter (K)	2.57	26.15
Period (λ)	5.5 cm	14 cm
Number of Periods (N)	50	14
Peak Field (B_0)	0.5 T	2 T
Length (L)	2.75 m	1.96 m
Photon Energy (ε)	1.33 KeV	5.32 KeV

Table 4. List of insertion device parameters

	Undulator	Wiggler
Q1, Q1M (before/after)	-0.5431/-0.34832	-1.3896/-0.9279
Q2, Q2M	1.3893/ 1.3617	2.0521/ 1.9379
Q3, Q3M	-1.6886/-1.6835	-1.8624/-1.8850

Table 5. Quadrupole strengths before and after α and tune matching

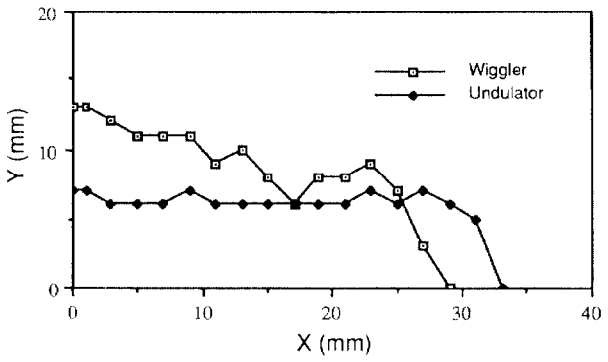

Figure 6. Dynamic apertures at high β_x ID symmetry point with one undulator and one wiggler in Table 4.

Appendix

With a different family of quadrupole strengths, a conventional type lattice functions (not a hybrid type) are obtained as shown in Figure 7. The parameters of this 12 period magnet lattice are shown Table 6, and momentum dependent tune shifts and a dynamic aperture without error are shown in Figures 8 and 9, respectively.

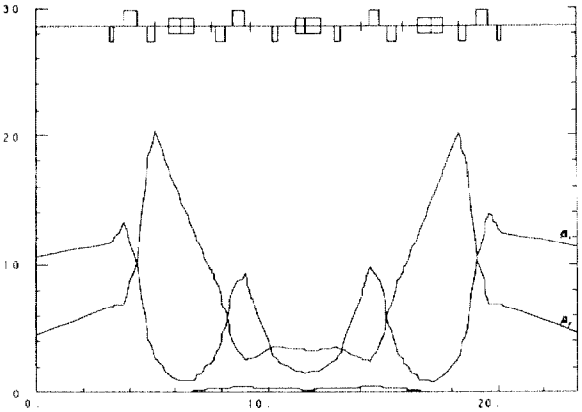

Figure 7. 12 period lattice functions over one cell.

Natural Emittance	11.9 ($nm \cdot rad$)
Natural Chromaticity (h/v)	-24.51/-16.98
Betatron Tunes (h/v)	14.28/8.18
Beta Functions (h/v)	
Maximum	13.6/20.15 (m)
Minimum	0.82/2.55 (m)
At ID symmetry point	11/4.61(m)
Beam Size at ID Sym. Pt. (high/low)	
Horizontal, σ_x	0.36 (mm)
Vertical ($r = 1$), σ_y	0.16(mm)
Energy Spread, σ_E	0.00068
Maximum Dispersion	0.48 (m)
Momentum Compaction	0.001791

Table 6. 12 period storage ring parameters at 2 GeV.

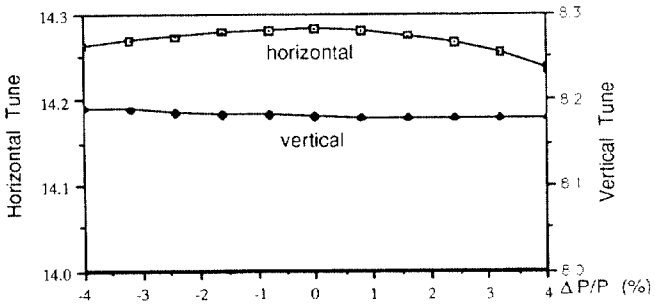

Figure 8. Tune shifts versus momentum of the 12 period lattice.

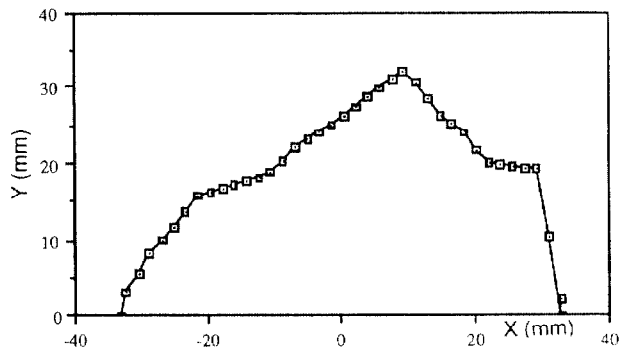

Figure 9. Dynamic aperture of the 12 period lattice without error.